Does Interfacial Vaporization of Organic Solvent Affect the Structure and Separation Properties of Polyamide RO membranes?

Lu Elfa Peng, [a] Yucen Jiang, [a] Lei Wen, [a] Hao Guo, [a] Zhe Yang, [a] Chuyang Y. Tang [a, *]

[a]Department of Civil Engineering, The University of Hong Kong, Pokfulam, Hong Kong SAR, China.

[*]Corresponding Authors:

Chuyang Y. Tang, tangc@hku.hk, +852 28591976

Graphic abstract

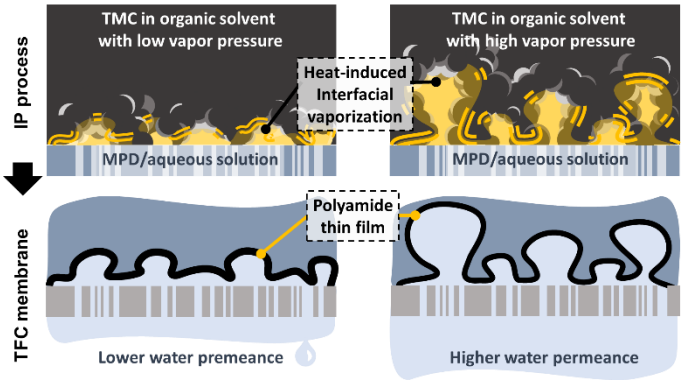

Abstract

Nanovoids in polyamide rejection layers of thin film composite (TFC) reverse osmosis (RO) membranes are responsible for their characteristic "ridge-and-valley" surface roughness and have profound impact on their separation performance. However, mechanisms leading to these void-containing roughness features remain poorly understood. The current work presents compelling evidence that vaporization of the organic solvent contributes to the formation of nanovoids during the exothermic interfacial polymerization (IP) process. We used a series of alkane solvents with systematically varying chain length and vapor pressure to prepare TFC membranes. Our study revealed that an organic solvent with higher vapor pressure generated more vapor during the IP reaction, which in turn resulted in larger size of the voids in the polyamide thin film and higher membrane water permeability. We further designed a strategy to suppress the vapor effect by preparing polyamide thin films at a free interface. This led to the disappearance of nanovoids and nearly identical membrane permeability regardless of the organic solvent used for the IP process, in good agreement of the weakened confinement to the organic vapor generated by interfacial heating. The current study provides new mechanistic insights to interpret the formation of the voids-containing morphology of TFC polyamide membranes, which would facilitate improved understanding of membrane transport mechanisms and better control of membrane structural features.

Keywords:

RO membrane, polyamide morphology, nanovoids, organic solvents, interfacial vaporization.

1. Introduction

Reverse osmosis (RO), the state-of-the-art technology for desalination and water reuse, relies on polyamide thin film composite (TFC) membranes [1-4]. The polyamide film is typically prepared on top of a porous substrate by the interfacial polymerization (IP, Fig. 1A) of *m*-phenylenediamine (MPD) and trimesoyl chloride (TMC), which occurs at an interface between two immiscible phases (e.g., water/hexane). It is widely believed that MPD monomers dissolved in the aqueous phase diffuse into the TMC-containing organic solvent to form the polyamide film [5-8]. This polyamide film, typically characterized with a "ridge-and-valley" surface morphology [9-11], encapsulates numerous nano-sized voids [12-17]. The nanovoids-containing roughness features are widely correlated with the separation performance of RO membranes [14-18]. However, mechanisms leading to these void-containing roughness features remain poorly understood.

It has been well documented that the roughness features can be strongly affected by the solvents used in the IP reaction [19-21]. For example, some studies investigated the use of co-solvents (e.g., alcohols [22, 23] and dimethyl sulfoxide [18, 24] in the aqueous phase or acetone [20, 21, 25] in the organic phase). This strategy often results in enlarged voids size [20, 26, 27], increased effective surface area [18, 24, 28] and/or reduced intrinsic film thickness [20, 27] (despite its larger apparent thickness [18, 26-28], Fig. 1B), which dramatically enhances membrane permeance. The effects of co-solvents on the morphology of polyamide are commonly explained by the enlarged IP reaction zone due to the increased miscibility of the two phases and/or the promoted diffusion of monomers from one phase to the other [18-21, 26]. Nevertheless, these studies do not provide direct mechanistic explanation on the formation of nanovoids.

Ma et al. [29] provided an alternative angle to understand the formation of nanovoids. According to these authors, the H^+ and heat generated by the IP reaction (Fig. 1A) can promote the interfacial degassing of CO_2 bubbles ($HCO_3^- + H^+ \xrightarrow{\Delta} CO_2\uparrow + H_2O$), which forms the nanovoids and shapes the morphology of the polyamide film [29-31]. Ukrainsky et al. [32] further investigated the interfacial heating phenomenon and reported temperatures as high as 90 ℃ near the IP reaction zone in some cases, which are well above the boiling point of many organic solvents (Fig. 2A). Therefore, we hypothesize that the vaporization of organic solvents, in addition to any degassing of CO_2, at the interface of the exothermic IP reaction promotes the formation of nanovoids (Fig. 1). Specifically, an organic solvent with a higher vapor pressure (or a lower boiling point) may result in larger and/or more voids.

In order to dissect the role of organic solvents, the current work employed four alkane-based solvents with systematically varying chain length and vapor pressure. We show that the morphology and separation performance of the prepared membranes are well correlated to the vapor pressure of the solvents. Additional polyamide films were also prepared at a substrate-free interface [33, 34] to further resolve the governing mechanisms. Our study provides compelling evidences on the role of interfacial vaporization of organic solvents towards the formation of surface roughness of polyamide membranes. These new mechanistic insights may improve the understanding of the structure-properties correlation of voids-containing TFC polyamide membranes and facilitate their better design and optimization.

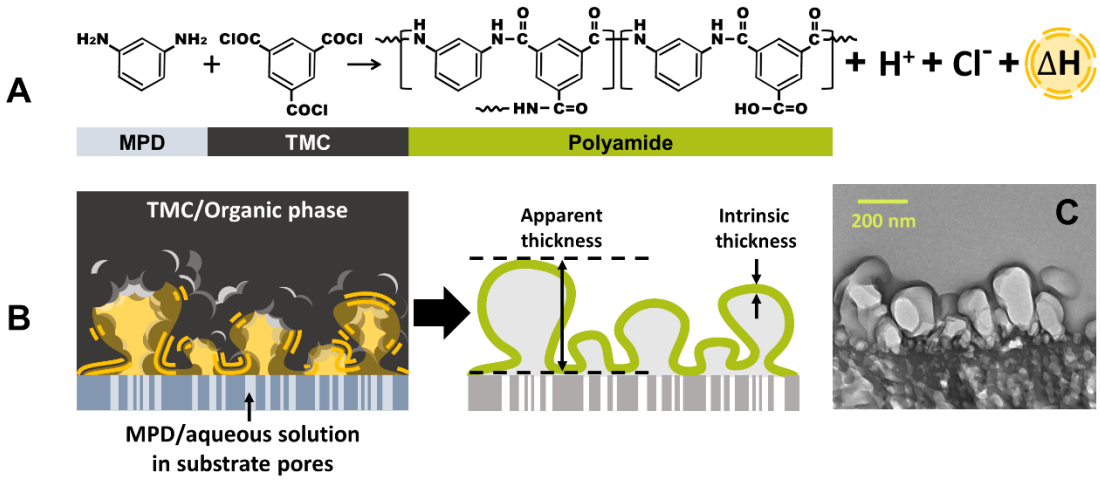

Fig. 1. IP reaction between MPD and TMC for the formation of a polyamide thin film. (A) The IP reaction generates acid and heat as byproducts. (B) Conceptual diagram of the interfacial vaporization during IP (left), which shapes the morphology of the polyamide thin film (right). (C) Transmission electron micrograph (cross-section) of a TFC polyamide membrane with nanovoids contained in the polyamide layer.

2. Materials and methods

2.1. Chemicals

Monomers MPD (99%) and TMC (98%), organic solvents n-octane, n-heptane, n-hexane purchased from Sigma-Aldrich and n-pentane (TCI) were used to perform the IP reaction and prepare polyamide thin films. Commercial polysulfone (PSf) substrates (MWCO 67 kDa, Vontron Technology) were used to prepare TFC membranes. Isopropanol (Dickmann) was used for pretreatment of the substrates. Glycerol (Dickmann) was used for sample treatment. Sodium chloride (NaCl, Dieckmann) was used for membrane performance tests. All aqueous solutions were prepared using Milli-Q water (Elix Essential).

2.2. Measurement of vapor generation

To evaluate the potential of organic solvents for vapor generation, an MPD solution (5 mL, 1 w/w%) was first placed in an airtight flask that was connected to a glass tube filled with an inked water column for better visualization (Fig. 2A). An organic solvent (0.1 mL, with or without 0.1 w/w% TMC) was then injected into the flask, and the vaporization of organic solvents were quantified based on the displacement of the water column. The volume displaced by vapor (V) can be calculated by the product of the displacement (Δh in cm, measured at 1 min after the addition of the organic phase) and the cross-sectional area of the glass tube (0.785 cm^2). All experiments were performed under ambient temperature (~ 25 ℃) and pressure (~ 1 bar).

To further analyze the composition of the gas/air mixture in the flask, a gas sampling bag in place of the water column was connected to the flask for collection of the mixture (Fig. 2A). In this set of tests, a larger volume of organic solvent (1 mL, with TMC) was

used each time to ensure sufficient vapor generation for sampling, while other conditions were kept identical to the water column displacement tests. The sample collected over the first minute was then analyzed using a gas chromatograph (GC, Trace 1310, Thermo Fisher, see Appendix C).

2.3. Partitioning of MPD in organic solvents

The diffusion of MPD from the water phase to the organic solvent and its solubility in the latter are commonly believed to strongly affect the morphology of a polyamide film [5, 7, 20, 35-37]. In this study, the partitioning of MPD between water and various organic solvents were evaluated. Specifically, an aqueous MPD solution (5 mL, 1 w/w%) was first placed in a centrifuge tube. An organic solvent (5 mL) was gently added to the top part of the tube, letting the solvent to contact the aqueous phase for 5 min. The MPD-dissolved solvent was then analyzed using an ultraviolet–visible spectrophotometer (UV/VIS, UH5300, Hitachi) at the wavelength of 294 nm to determine the MPD concentration (Appendix D) [19, 27, 38]. During the above partitioning test, the concentration of MPD in the aqueous phase remained nearly constant since its solubility (36.1 g/100mL [39]) in water is several orders of magnitude higher than those in the organic solvents.

2.4. Preparation of TFC polyamide membranes

PSf substrates were presoaked with 25 v/v% isopropanol for 1h under moderate shaking [40, 41], followed by thorough rinsing by Milli-Q water. A conventional TFC membrane was prepared by directly performing IP between MPD (1 w/w% [42, 43], dissolved in water) and TMC (0.1 w/w%, dissolved in octane, heptane, hexane or pentane) on the substrate. Briefly, the MPD solution was first applied to impregnate a

PSf substrate for 2 min. After removing the excess MPD solution by a rubber roller, the substrate was then soaked in the TMC solution for 1 min to form the polyamide layer. The resulted polyamide membrane was then rinsed by the same organic solvent and was placed in a 50 °C water bath for 10 min for further polymerization. Since a main objective of this study was to investigate the role of solvent on the polyamide morphology, water bath treatment [44-46] was used instead of oven drying to avoid severe collapse of the roughness features [33, 45]. The prepared TFC membranes were named as TFC-solvent, e.g., TFC-octane for the one prepared using octane.

2.5. Preparation of freestanding polyamide thin films

To further resolve the role of organic solvents, we prepared polyamide thin films at a free interface [8, 47-49]. According to existing literature [33, 34], gas bubbles released during the IP reaction can easily escape from the free interface due to the lack of confinement. This would suppress the effect of interfacial-vaporization/degassing on the polyamide morphology. We followed the method of Song et al. [33] to prepare polyamide films at the free interface. Briefly, a 1 w/w% MPD solution and a 0.1 w/w% TMC dissolved in an organic solvent were allowed to react for 1 min. The resulted polyamide film was then loaded onto the PSf substrate under assistance of a vacuum suction. The corresponding membrane is denoted as PAfi-solvent according to the type of solvent used. After the removal of excess TMC solution, the membrane was rinsed by the same organic solvent before further use.

2.6. Membrane characterization

Field-emission scanning electron microscopy (FE-SEM, S-4800, Hitachi) operated at an accelerating voltage of 5.0 kV was used to characterize the surface morphology of

membranes. All samples were dried and sputter coated with a thin layer of gold before SEM characterization. Transmission electron microscopy (TEM, CM100, Philips) operated at an accelerating voltage of 100 kV was used to resolve the cross-sectional structure of membranes. Samples were soaked in 10 v/v% glycerol/water for 1 h [33] and dried before TEM characterization. X-ray photoelectron spectroscopy (XPS, ULVAC-PHI X-tool) with a spectra range of 0-1400 eV was employed to analyze the elemental composition of membrane surfaces.

2.7. Membrane separation performance evaluation

Water flux and salt (NaCl) rejection of the membranes were tested using a laboratory-scale cross-flow RO filtration system as reported in our previous work [31]. Each membrane coupon with effective filtration area of 12.0 cm^2 was pre-compacted at 17.0 bar for 2 h. The test was conducted at 15.5 bar using a 2000 ppm NaCl feed solution with a cross-flow velocity of 22.4 cm/s under room temperature (~25 °C). The water flux J_v and permeability A are calculated by:

$$J_v = \frac{\Delta m}{\Delta t \times a \times \rho} \quad (1)$$

$$A = \frac{J_v}{\Delta P - \Delta \pi} \quad (2)$$

where Δm is the mass of permeate over a time interval of Δt, a is the effective membrane area, ρ is the density of water, ΔP is the transmembrane pressure, and $\Delta \pi$ is the transmembrane osmotic pressure. NaCl rejection (R) was calculated by:

$$R = \frac{C_f - C_p}{C_f} \times 100\% \quad (3)$$

where C_f and C_p are NaCl concentrations in the feed and the permeate respectively, which were determined based on conductivity measurements (Ultrameter II, Myron L).

3. Results and discussion

3.1. Vaporization of organic solvents during IP

As the chain length of an alkane solvent decreases, its vapor pressure increases and boiling point reduces (Fig. 2B). In this study, we evaluated the amount of vapor generation by adding an organic solvent (with or without TMC) into an airtight flask containing an MPD solution and measuring the induced volume displacement (Fig. 2A). For the blank tests (without TMC), solvents with higher vapor pressure (and lower boiling point) resulted in more vapor generation (Fig. 2C). With the inclusion of TMC to induce the IP reaction, the displaced volume was further increased. This can be explained by the heat generated in the exothermic reaction (Fig. 1A) to promote further vaporization of the solvents. This effect was most obvious for pentane that has the lowest boiling point.

To further analyze the composition of the vapor/air mixture in the flask after the addition of TMC dissolved solvent, we analyzed the mixture by a GC (Appendix C). The concentration of pentane in the mixture was nearly three order of magnitude higher than that of hexane (Fig. 2D), while the concentrations of heptane and octane were below detection. The generation of vapor also reduced the fraction of N_2 that was originally present in the headspace. The GC results provide consistent evidence on the vaporization of organic solvents during the IP reaction.

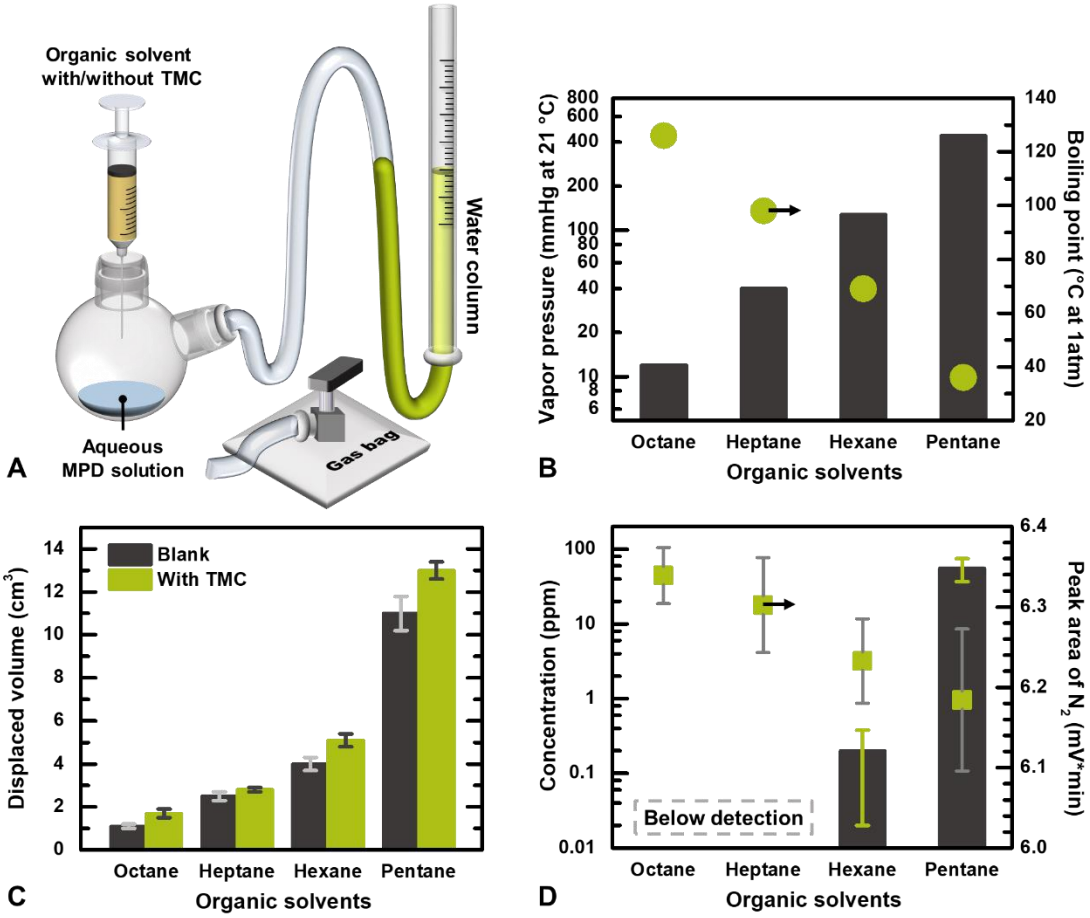

Fig. 2. (A) Schematic diagram of the setup for measurement of vapor generation, (B) vapor pressure and boiling point of the organic solvents [50] ; (C) the displaced volume induced by each organic solvent without (blank) or with TMC in the airtight flask prefilled with a MPD solution, and (D) the contents of organic solvents and N_2 in the vapor/air mixture based on GC results (the peak area of N_2 in ambient air is 6.36 ± 0.11 mV*min).

3.2. Interfacial vaporization tunes the voids features

SEM surface micrographs (top panel of Fig. 3) present typical "ridge-and-valley" roughness features that are commonly reported for polyamide membranes [14, 15, 17] . Compared to TFC-octane, TFC-pentane had greater number of large "leaves". The TEM photos further highlighted the differences. From TFC-octane to TFC-pentane, the voids encapsulated in the polyamide layer became more obvious and larger, which correlates well with the greater tendency of pentane to vaporize (Fig. 2). Correspondingly, TFC-pentane also had the greatest apparent thickness (~ 334 nm as shown in Appendix E), largely due to the presence of bigger-size voids. This observation is consistent with our hypothesis that interfacial vaporization of organic solvent can enhance the formation of nanovoids and shape the surface roughness of polyamide films. The IP reaction of polyamide is exothermic and releases heat, which promotes vaporization of organic solvent at the reaction interface (Fig. 1). With the mesoporous substrate providing resistance to prevent its escape (i.e., the confinement effect [33, 34]), the vapor generated at the reaction interface is encapsulated between the substrate and the nascent polyamide film, leading to the formation of nanovoids inside the polyamide film. Consequently, greater vapor generation for more volatile organic solvent promotes more extensive nanovoids formation.

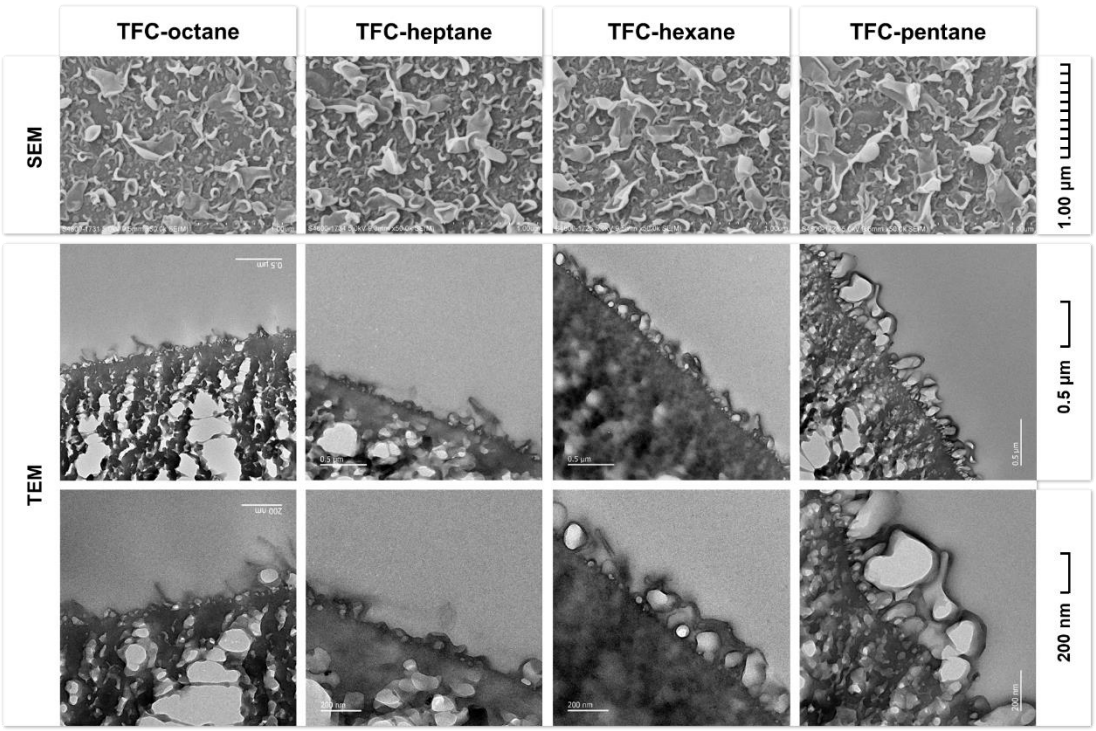

Fig. 3. SEM top views and TEM cross-sections of the TFC membranes.

To further dissect the formation mechanism of nanovoids, we prepared additional polyamide films by performing IP at a free interface (PAfi). According to previous works by Song and Peng et al. [33, 34, 51], the lack of substrate would allow degassed nanobubbles [29-31] to freely escape from the reaction interface due to the lack of confinement by the substrate. Therefore, if the formation of nanovoids are driven by interfacial vaporization/degassing, performing IP reaction at a free interface would largely suppress the ability of degassed nanobubbles to induce the voids-containing "ridge-and-valley" morphology [33]. In contrast, if the formation of nanovoids are mainly regulated by the solubility of MPD in the organic phase, we would expect similar "ridge-and-valley" surface morphologies for PAfi membranes.

Fig. 4 presents the SEM surface morphology and TEM cross-sections of the PAfi membranes. Compared to the TFC membranes prepared on the PSf substrate (Fig. 3),

the PAfi membranes generally gave much flatter surface morphologies with fewer leave-like features (Fig. 4). The "ridge-and-valley" roughness features were nearly absent, which is consistent with the interfacial vaporization theory [8, 33, 47]. In addition, the TEM micrographs (Fig. 4) present less obvious differences between the cross-sectional morphologies of the PAfi membranes formed with different solvents, with the nanovoids found in conventional TFC polyamide membranes largely disappeared. The absence of voids corresponds well to the weakened confinement effect to allow the escape of vapor. This observation rules out the MPD solubility effect as a dominant mechanism in shaping the polyamide morphology.

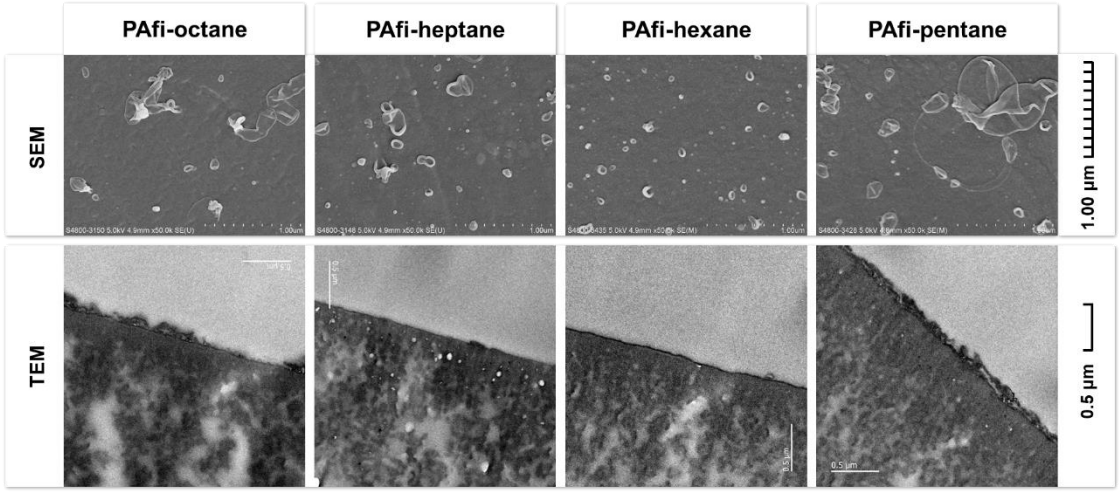

Fig. 4. SEM top views and TEM cross-sections of the PAfi membranes.

3.3. Separation performance of membranes

Fig. 5 presents the separation performance of the TFC and PAfi membranes. Although the TFC membranes had comparable rejections, their water permeability increased from 1.0 ± 0.3 $Lm^{-2}h^{-1}bar^{-1}$ for TFC-octane to 1.7 ± 0.2 $Lm^{-2}h^{-1}bar^{-1}$ for TFC-pentane (Fig. 5A). This enhancement in permeability can be explained by their voids-containing roughness features in Fig. 3. The larger voids of TFC-pentane correspond to greater

roughness of the polyamide film thus a greater effective surface area for water filtration [18, 24, 28]. In addition, the larger voids could also provide enhanced gutter effect [16, 49] and reduced intrinsic thickness [27] of the polyamide film to allow more efficient water transport through the polyamide rejection layer.

In contrast to the obvious differences in water permeability of the various TFC membranes (Fig. 5A), Fig. 5B shows only marginal differences between the PAfi membranes formed at free interfaces (Fig. 5B). Noticeably, we could not observe the enhancement effect on permeability for PAfi membranes formed with more volatile organic solvents. This observation is consistent with the interfacial vaporization theory and could be readily explained by the ineffectiveness in forming nanovoids (Fig. 4) due to the weakened confinement effect [33, 34]. Indeed, all the PAfi membranes had similar permeability to that of TFC-octane, a TFC membrane that had diminished void formation (Fig. 3) due to the low vapor pressure of octane (Fig. 2B). Even though TFC-octane contained some voids, the relatively smaller size of these voids may explain their ineffectiveness in water transport. A recent study [51] also reveals the critical importance of the connectivity of the nanovoids to the substrate pores on water transport. The ineffective voids formation may weaken such connectivity, a topic that requires further investigation.

In this study, the PAfi membranes generally presented higher rejections compared to the TFC membranes. This result is consistent with the lower O/N ratios (an indication of higher crosslinking degree) for the PAfi membranes (Table F1 in Appendix F), which can possibly be attributed to the greater MPD supply from the bulk aqueous solution for the case of PAfi. This enhanced "MPD reservoir" effect [34, 48, 52] would

potentially allow a more complete IP reaction. Alternatively, the generated H^+ in the reaction could also be more readily neutralized by the alkaline MPD solution [31], which favors dense polyamide films with higher rejection.

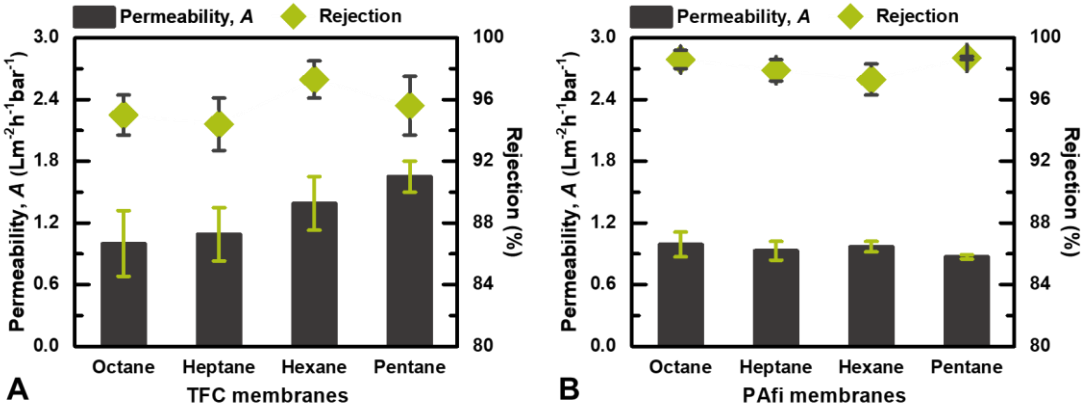

Fig. 5. Separation performance of (A) the TFC membranes and (B) the PAfi membranes.

3.4. Mechanistic insights

Conventional wisdom generally attributes improved roughness formation in polyamide membranes to enhanced diffusion of MPD monomers and/or their greater solubility in the organic phase [7, 20, 36, 37]. Fig. 6 presents the amount of MPD that partitions from an aqueous solution into various organic solvents. Clearly, greater amount of MPD had diffused to and dissolved in the shorter-chain alkanes (pentane > hexane > heptane ~ octane). This trend appears to be consistent with the rougher surfaces observed for TFC-pentane and TFC-hexane (Fig. 3). The explanation is also apparently supported by the observed greater roughness formation with increased MPD concentrations under otherwise identical IP conditions [8, 36]. Nevertheless, the diffusion/solubility effect would have resulted in a similar trend for the PAfi membranes formed with different organic solvents, which contradicts with the experimental observations (Fig. 4). Indeed, had the roughness formation been

dominated by the diffusion/solubility effect, one would expect a rougher polyamide formed at a free interface compared to that formed on a substrate as a result of greater availability of MPD (and thus increased effective MPD concentration in the organic phase) for the former case [36]. In this respect, the interfacial vaporization/degassing theory provides more consistent explanations to the formation of nanovoids-containing surface roughness features [29, 33, 34, 51], the effect of the availability and solubility of dissolved CO_2 [29-31], the vapor pressure of organic solvents (Fig. 2B), and the confinement effects [33, 34]. Despite the dominant role of the interfacial vaporization/degassing mechanism, the MPD solubility effect could still play an indirect role: greater MPD supply would result in more heat generation during the IP reaction (Fig. 1A) and thus promotes interfacial vaporization/degassing [29]. This indirect effect explains why increasing MPD concentration would form rougher polyamide surfaces. Future studies need to consider both the direct nanovoid forming mechanisms (e.g., degassing of CO_2 and vaporization of organic solvent) as well as the indirect effects (e.g., MPD supply) for tailoring membrane morphology and optimizing their separation performance.

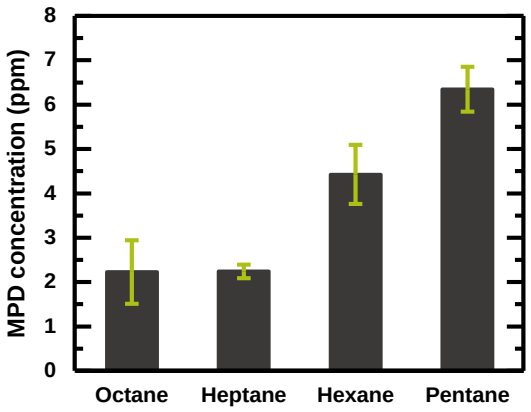

Fig. 6. MPD concentration in various organic solvents. For each organic solvent, its MPD concentration was measured after it had contacted a 1 w/w% aqueous MPD

solutions for 5 min.

4. Conclusions

The current study reveals a new mechanism, interfacial vaporization of organic solvent that can contribute to nanovoid formation and regulate the polyamide morphology. More extensive voids in the polyamide layer and greater membrane permeability can be achieved by promoting the vaporization of organic solvent during the exothermic IP reaction, e.g., by using an organic solvent with higher vapor pressure. This mechanism may also provide explanation to the commonly reported enlargement effect of roughness features upon the addition of volatile co-solvents such as acetone [20, 26, 53], alcohols [22, 23], and diethyl ether [53] although additional systematic studies are required to confirm this explanation. Future studies need to further investigate if water would be vaporized or even boiled locally given the high temperature at the IP interface [32]. Other secondary effects, such as the heat dissipation via vaporization, may need be accounted for. Our work provides a new framework to interpret the formation of the polyamide morphology. The interfacial vaporization theory, complementary to our earlier reports on interfacial CO_2 degassing [29-31] and confinement effects [33, 34, 51], opens a new door towards controllable membrane nano-architectures for more efficient separation in various environmental applications.

Acknowledgments

We thank Mr. Pengfei Sun from Korea University for providing XPS analysis. We also thank Professor Xiaoyan Li's laboratory on the assistance on gas chromatography analysis. The work is partially supported by the Research Grants Council of the Hong Kong Special Administration Region, China (SRFS2021-7S04; GRF HKU 17204220).

Appendix A. Physical properties of organic solvents

The important physical properties of organic solvents that boiling point, vapor pressure, specific gravity, surface tension and viscosity are summarized in Table A1.

Table A1. Common physical properties of water and the organic solvents in this study. (adapted from Ref. [50])

	Water	Octane	Heptane	Hexane	Pentane
Boiling point (℃ at 1 atm)	100	126	98	69	36
Vapor pressure (mmHg at 21 ℃)	2.3	12	40	128	442
Density (g/cm^3) *	1	0.703	0.664	0.659	0.626
Surface tension (mN/m)	72.8	21.7	19.3	18.4	16.0
Absolute viscosity (cP at 25 ℃)	0.89	0.51	0.41	0.31	0.24

Note: * The density is measured at 4 °C for water and 20 °C for the organic solvents.

Appendix B. Water column for measurement of vapor generation

Fig. B1 shows the photos of water column displacement after injecting an organic solvent (with or without TMC) in an airtight flask prefilled with an aqueous MPD solution. The red dotted line is the initial position (0 cm) of the water column. For each test, injecting the organic solvent with TMC induced greater displacement than that without TMC. From octane to pentane with increased vapor pressure, greater displacement was obtained.

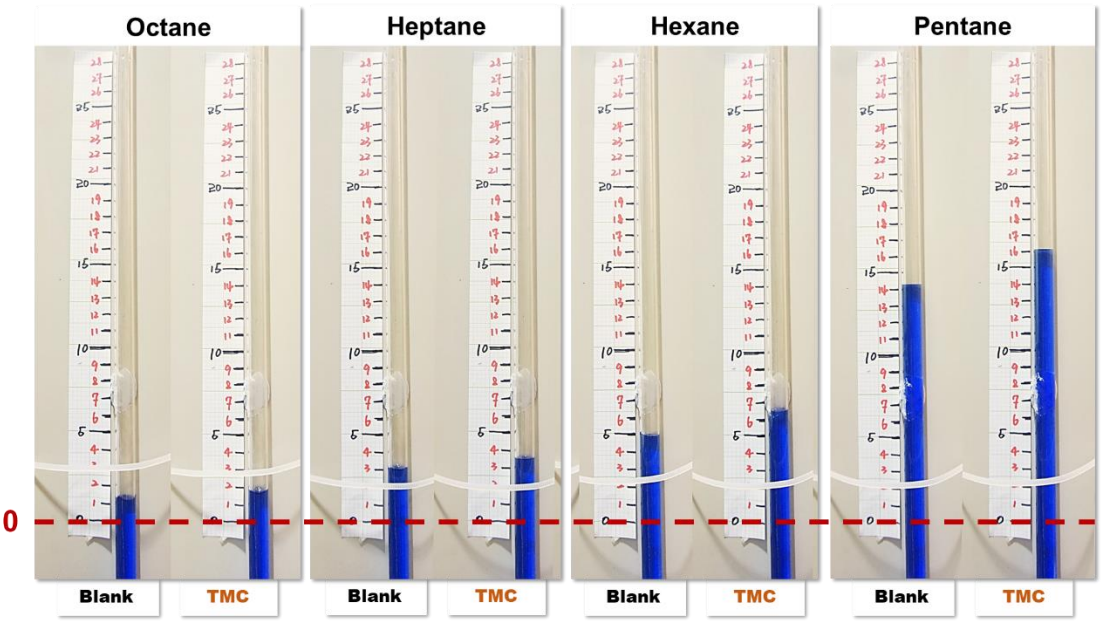

391

392 **Fig. B1.** Photos of the water column displacement after injecting an organic solvent
393 (with or without TMC) in an airtight flask containing an aqueous MPD solution.

394

395 **Appendix C. Gas chromatograph (GC) for measurement of air mixture**

396 The GC (Thermo scientific Trace 1310) was equipped with a capillary column TG-
397 BOND Q (length 30m; Diameter 0.53mm; film thickness 20um) and a TCD detector to
398 quantify nitrogen gas (N_2). Another identical column with an FID detector was used to
399 quantify organic solvents. The sample injection volume was 50 uL. The carrier gas was
400 helium at a constant speed of 4 ml/min for N_2 and 6ml/min for solvents, with split ratio
401 of 3 for N_2 and no split mode for solvents. The temperatures for N_2 quantification were
402 120^{o}C for injector, 60^{o}C for oven, 200^{o}C for detector, and 250^{o}C for filament. Those
403 for organic solvents were 120^{o}C for injector, 150^{o}C for oven, 250^{o}C for detector. N_2
404 gas with 99.98% purity was taken as a standard to determine its residence time.
405 Standard pentane, hexane, heptane, and octane were injected to determine their relative
406 residence time and concentration, respectively. Table C1 shows the results from GC.

407

Table C1. Gas chromatograph (GC) results on the peak area and peak height of N_2 and organic solvents in each sample of gas/air mixture.

Peak height (mV)			
	N_2	CO_2	Solvent
Ambient air	104.65 ± 1.51	0.063 ± 0.006	-
Octane	103.89 ± 0.33	0.065 ± 0.007	Below detection
Heptane	102.53 ± 0.84	0.067 ± 0.006	Below detection
Hexane	100.97 ± 3.56	0.070 ± 0.008	3.11 ± 2.53
Pentane	97.45 ± 3.50	0.084 ± 0.043	2041.14 ± 561.68
Peak area (mV*min)			
	N_2	CO_2	Solvent
Ambient air	6.36 ± 0.11	0.0040 ± 0.0005	-
Octane	6.34 ± 0.03	0.0045 ± 0.0008	Below detection
Heptane	6.30 ± 0.06	0.0044 ± 0.0005	Below detection
Hexane	6.23 ± 0.05	0.0047 ± 0.0012	0.25 ± 0.22
Pentane	6.18 ± 0.09	0.0054 ± 0.0024	70.55 ± 23.99

The ratio between peak areas of CO_2 and N_2 can indicate the relative content of CO_2 in each sample (Table C2). In the current study, CO_2 was contributed from both the air in the headspace and that degassed during the IP reaction [29]. In contrast, N_2 was solely attributed from the air in the headspace. Using ambient air as a control, the degassed CO_2 can be evaluated. Generally, the CO_2 content of the pentane-based IP reaction was higher than those with solvents of lower vapor pressures. This can be explained by the greater availability MPD monomers for the IP reaction (Fig. 6) and thus more heat released to drive the degassing of CO_2. Nevertheless, CO_2 degassing alone can hardly enlarge the voids by around an order of magnitude (i.e., TFC-pentane vs. TFC-octane in Fig. 3). Instead, interfacial vaporization of solvent works synergistically with interfacial degassing of CO_2 to cause the extensive formation of roughness features in the current study.

Table C2. The relative content of CO_2 in each sample of gas/air mixture calculated based on the GC results of the peak areas.

Peak area (mV*min)			CO_2/ N_2 ($\times 10^{-4}$)	
	N_2	CO_2	Total CO_2	Degassed CO_2
Ambient air	6.36 ± 0.11	0.0040 ± 0.0005	6.29	-
Octane	6.34 ± 0.03	0.0045 ± 0.0008	7.10	0.81
Heptane	6.30 ± 0.06	0.0044 ± 0.0005	6.98	0.69
Hexane	6.23 ± 0.05	0.0047 ± 0.0012	7.54	1.25
Pentane	6.18 ± 0.09	0.0054 ± 0.0024	8.74	2.45

Appendix D. MPD concentration in organic solvents

The concentration of MPD dissolved in the series of organic solvents were calculated based on the standard curve (Fig. D1) between the concentration (C, 1~25 ppm) and absorbance (Abs) of MPD:

$$Abs = 0.0173C - 0.0003 \ (R^2 \text{ is} > 0.99) \quad (1)$$

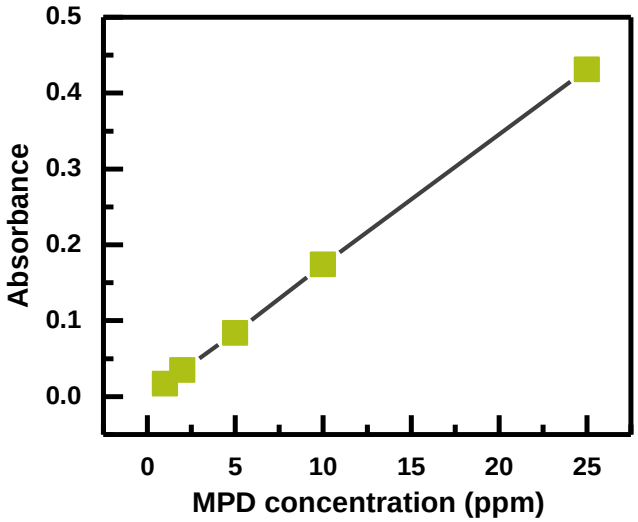

Fig. D1. Standard curve for MPD concentration measurement by an ultraviolet–visible (UV) spectrophotometer at the wavelength of 294 nm.

Appendix E. TEM micrographs marked with apparent and intrinsic thickness

Fig. E1 displays the TEM micrographs marked with the apparent and intrinsic thickness. The membrane apparent thickness increased from ~125 nm for TFC-octane to ~334nm for TFC-pentane. The intrinsic thickness was generally in the range of 9-69 nm for TFC-octane, 13-41 nm for TFC-heptane, 9-65 nm for TFC-hexane, and 7-36 nm for TFC-pentane. It is important to note that, due to the limited resolution of TEM micrographs and the inherent limitation of TEM sample preparation (Fig. E2), it was difficult to accurately quantify the intrinsic thickness of polyamide thin films. For example, the finite thickness of the TEM sample (typically on the order of 100 nm) could result in an overestimation of intrinsic thickness (Fig. E2).

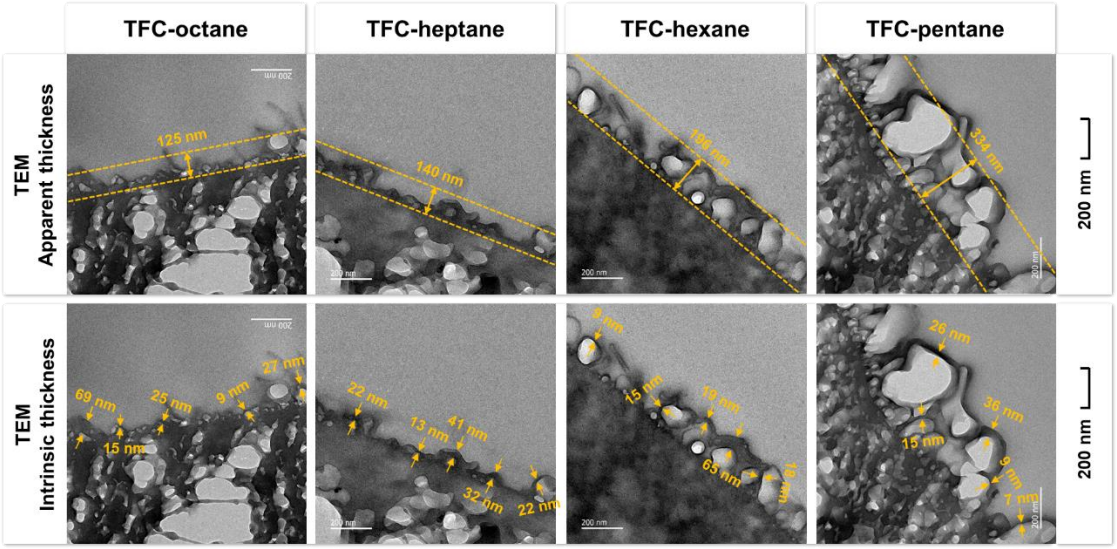

Fig. E1. TEM cross-sections of the TFC membranes with marked thickness.

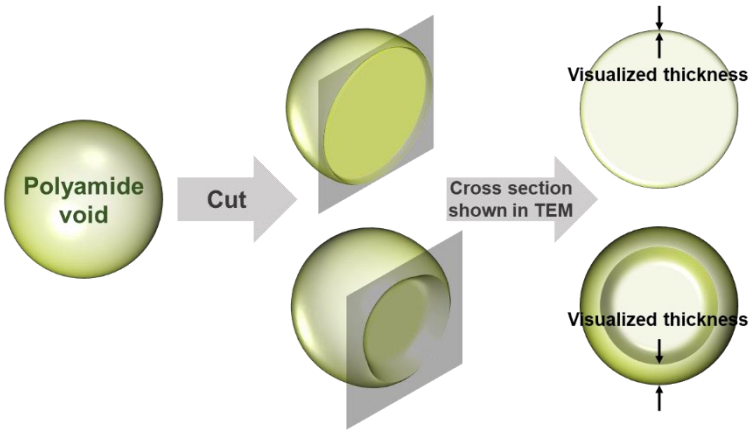

Fig. E2. Diagram of the cross section of a polyamide void for TEM after sample cutting.

Appendix F. XPS results

Based on XPS results of membranes, the ratios between O and N (O/N) were calculated, with a lower O/N ratio indicating a more cross-linked polyamide layer. The PAfi membranes generally gave lower O/N ratios than the TFC counterparts, which indicates more extensive cross-linking of the PAfi membranes. Indeed, O/N ratios of PAfi membranes were below 1, which may be explained by the excess supply of MPD monomers at the free interface to result in excess amine-terminal groups at the polyamide surface. In the current study, we did not observe a clear trend on the effect of solvents on the O/N ratio.

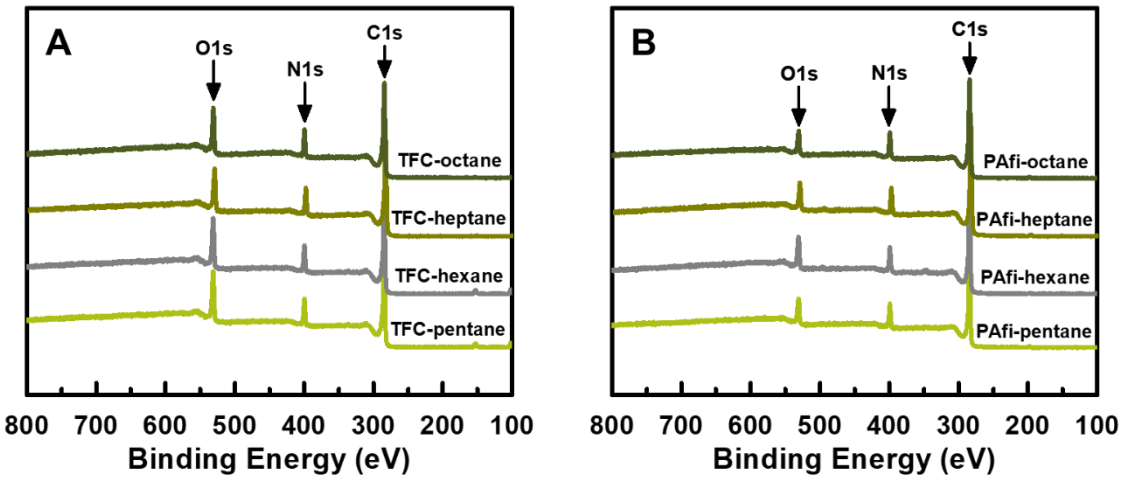

C

Membranes	O/N ratio	Membranes	O/N ratio
TFC-octane	1.49 ± 0.06	PAfi-octane	0.68 ± 0.04
TFC-heptane	1.37 ± 0.07	PAfi-heptane	0.80 ± 0.04
TFC-hexane	1.66 ± 0.08	PAfi-hexane	1.04 ± 0.01
TFC-pentane	1.60 ± 0.09	PAfi-pentane	0.85 ± 0.03

Fig F1. XPS spectrum of TFC (A) and PAfi (B) membranes with the calculated O/N ratio (C) based on XPS results.

Appendix G. Additional TFC membranes prepared using equal-w/v% concentration of TMC

In the current study, TFC membranes were generally prepared using equal concentration of TMC based on w/w%. However, due to the different densities of the organic solvents (e.g., 0.626 g/cm^3 for pentane and 0.703 g/cm^3 for octane, see Table A1 in Appendix A), the corresponding volumetric concentrations can be significantly different. To address this issue, two additional membranes were prepared: TFC-pentane-v and TFC-octane-v, both using 0.1 w/v% TMC. Fig. G1 presents the micrographs of these membranes. From the TEM cross-sections, TFC-pentane-v had larger voids in its polyamide layer compared to TFC-octane-v. Furthermore, TFC-pentane-v had better separation performance (permeability of 1.5 ± 0.1 Lm^{-2}h^{-1}bar^{-1} and

NaCl rejection of 97.3 ± 1.1%) than TFC-octane-v (permeability of 1.0 ± 0.2 $Lm^{-2}h^{-1}bar^{-1}$ and NaCl rejection of 95.9 ± 0.5%). These trends are consistent with those observed for their counterparts (TFC-pentane vs. TFC-octane) prepared using equal-w/w% concentration.

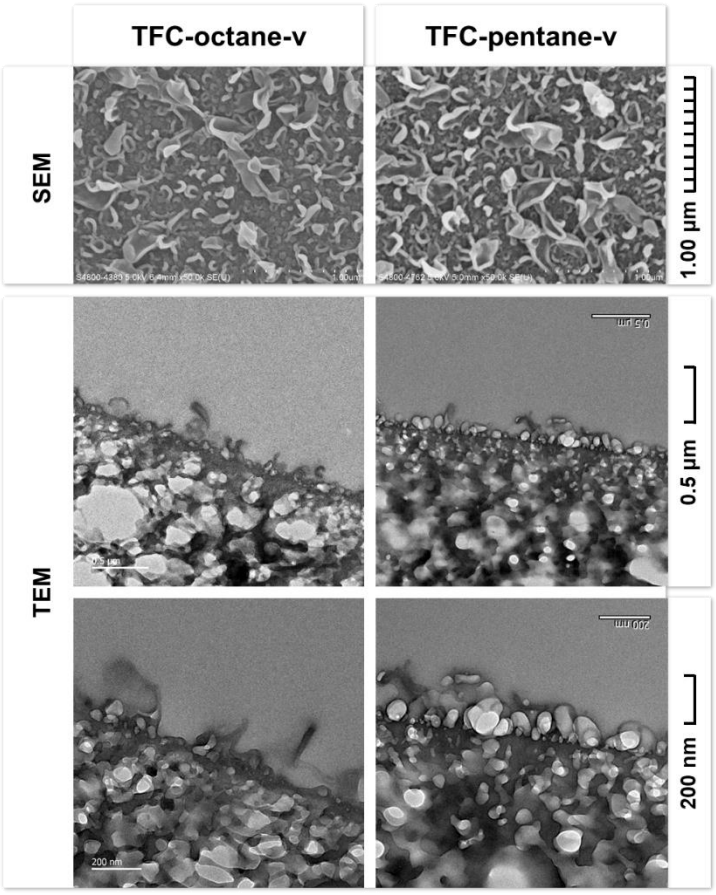

Fig. G1. SEM top views and TEM cross-sections of TFC-pentane-v and TFC-octane-v (prepared using 0.1 w/v% TMC).

Appendix H. Performance of some lab-prepared and commercial TFC RO membranes

The performance of TFC-hexane (i.e., permeability of 1.4 ± 0.3 $Lm^{-2}h^{-1}bar^{-1}$ and NaCl rejection of 97.3 ± 1.2%) in this work is comparable to many lab-prepared TFC membranes even some commercial membranes as show in Table H1. It is worthwhile to note that the relatively low NaCl rejection for the commercial RO membranes (SW30 and SWHR) was due to the relatively low testing pressure [4].

Table H1. Performance of lab-prepared TFC membranes and commercial RO membranes in literature.

Membranes	Permeability ($Lm^{-2}h^{-1}bar^{-1}$)	NaCl Rejection (%)	Applied pressure (bar)	Feed NaCl concentration (ppm)	Remark
TFC-octane	1.0 ± 0.3	95.0 ± 1.3	15.5	2000	This study
TFC-heptane	1.1 ± 0.3	94.4 ± 1.7	15.5	2000	This study
TFC-hexane	1.4 ± 0.3	97.3 ± 1.2	15.5	2000	This study
TFC-pentane	1.7 ± 0.2	95.6 ± 1.9	15.5	2000	This study
TFC	1.1 ± 0.1	97.0 ± 0.5	10	500	[54]
TFC	0.8 ± 0.04	93.4 ± 1.1	12.4	2000	[55]
IP-PA	0.8 ± 0.2	96.8 ± 0.9	15.5	2000	[56]
SW30	1.0 ± 0.1	96.0 ± 0.2	10	500	[54]
SWHR	0.9 ± 0.1	92.0 ± 1.9	12.4	2000	[55]

References

[1] M. Elimelech, W.A. Phillip, The future of seawater desalination: energy, technology, and the environment, Science, 333 (2011) 712-717.

[2] C.Y. Tang, Z. Yang, H. Guo, J.J. Wen, L.D. Nghiem, E. Cornelissen, Potable Water Reuse through Advanced Membrane Technology, Environ. Sci. Technol., 52 (2018) 10215-10223.

[3] M. Qasim, M. Badrelzaman, N.N. Darwish, N.A. Darwish, N. Hilal, Reverse osmosis desalination: A state-of-the-art review, Desalination, 459 (2019) 59-104.

[4] Z. Yang, H. Guo, C.Y.Y. Tang, The upper bound of thin-film composite (TFC) polyamide membranes for desalination, J. Membr. Sci., 590 (2019) 117297.

[5] P.W. Morgan, S.L. Kwolek, Interfacial polycondensation. II. Fundamentals of polymer formation at liquid interfaces, J. Polym. Sci., 40 (1959) 299-327.

[6] J.E. Cadotte, Evolution of composite reverse osmosis membranes, in, ACS Publications, 1985.

[7] A.K. Ghosh, E.M.V. Hoek, Impacts of support membrane structure and chemistry on polyamide–polysulfone interfacial composite membranes, J. Membr. Sci., 336 (2009) 140-148.

[8] S. Karan, Z.W. Jiang, A.G. Livingston, Sub-10 nm polyamide nanofilms with ultrafast solvent transport for molecular separation, Science, 348 (2015) 1347-1351.

[9] M. Elimelech, X.H. Zhu, A.E. Childress, S.K. Hong, Role of membrane surface morphology in colloidal fouling of cellulose acetate and composite aromatic polyamide reverse osmosis membranes, J. Membr. Sci., 127 (1997) 101-109.

[10] I.J. Roh, A.R. Greenberg, V.P. Khare, Synthesis and characterization of interfacially polymerized polyamide thin films, Desalination, 191 (2006) 279-290.

[11] C.Y.Y. Tang, Y.N. Kwon, J.O. Leckie, Probing the nano- and micro-scales of reverse osmosis membranes - A comprehensive characterization of physiochemical properties of uncoated and coated membranes by XPS, TEM, ATR-FTIR, and streaming potential measurements, J. Membr. Sci., 287 (2007) 146-156.

[12] F.A. Pacheco, I. Pinnau, M. Reinhard, J.O. Leckie, Characterization of isolated polyamide thin films of RO and NF membranes using novel TEM techniques, J. Membr. Sci., 358 (2010) 51-59.

[13] H. Yan, X. Miao, J. Xu, G. Pan, Y. Zhang, Y. Shi, M. Guo, Y. Liu, The porous structure of the fully-aromatic polyamide film in reverse osmosis membranes, J. Membr. Sci., 475 (2015) 504-510.

[14] L. Lin, R. Lopez, G.Z. Ramon, O. Coronell, Investigating the void structure of the

polyamide active layers of thin-film composite membranes, J. Membr. Sci., 497 (2016) 365-376.
[15] M.M. Kłosowski, C.M. McGilvery, Y. Li, P. Abellan, Q. Ramasse, J.T. Cabral, A.G. Livingston, A.E. Porter, Micro-to nano-scale characterisation of polyamide structures of the SW30HR RO membrane using advanced electron microscopy and stain tracers, J. Membr. Sci., 520 (2016) 465-476.
[16] M.C.Y. Wong, L. Lin, O. Coronell, E.M.V. Hoek, G.Z. Ramon, Impact of liquid-filled voids within the active layer on transport through thin-film composite membranes, J. Membr. Sci., 500 (2016) 124-135.
[17] F. Pacheco, R. Sougrat, M. Reinhard, J.O. Leckie, I. Pinnau, 3D visualization of the internal nanostructure of polyamide thin films in RO membranes, J. Membr. Sci., 501 (2016) 33-44.
[18] S.Y. Kwak, S.G. Jung, S.H. Kim, Structure-motion-performance relationship of flux-enhanced reverse osmosis (RO) membranes composed of aromatic polyamide thin films, Environ. Sci. Technol., 35 (2001) 4334-4340.
[19] A.K. Ghosh, B.-H. Jeong, X. Huang, E.M.V. Hoek, Impacts of reaction and curing conditions on polyamide composite reverse osmosis membrane properties, J. Membr. Sci., 311 (2008) 34-45.
[20] C. Kong, M. Kanezashi, T. Yamomoto, T. Shintani, T. Tsuru, Controlled synthesis of high performance polyamide membrane with thin dense layer for water desalination, J. Membr. Sci., 362 (2010) 76-80.
[21] C. Kong, T. Shintani, T. Kamada, V. Freger, T. Tsuru, Co-solvent-mediated synthesis of thin polyamide membranes, J. Membr. Sci., 384 (2011) 10-16.
[22] M. Hirose, H. Ito, M. Maeda, K. Tanaka, Highly permeable composite reverse osmosis membrane, method of producing the same, and method of using the same, in, Google Patents, 1997.
[23] B. Khorshidi, B. Soltannia, T. Thundat, M. Sadrzadeh, Synthesis of thin film composite polyamide membranes: Effect of monohydric and polyhydric alcohol additives in aqueous solution, J. Membr. Sci., 523 (2017) 336-345.
[24] S.H. Kim, S.Y. Kwak, T. Suzuki, Positron annihilation spectroscopic evidence to demonstrate the flux-enhancement mechanism in morphology-controlled thin-film-composite (TFC) membrane, Environ. Sci. Technol., 39 (2005) 1764-1770.
[25] T. Kamada, T. Ohara, T. Shintani, T. Tsuru, Controlled surface morphology of polyamide membranes via the addition of co-solvent for improved permeate flux, J. Membr. Sci., 467 (2014) 303-312.

570 [26] S.-J. Park, S.J. Kwon, H.-E. Kwon, M.G. Shin, S.-H. Park, H. Park, Y.-I. Park, S.-
571 E. Nam, J.-H. Lee, Aromatic solvent-assisted interfacial polymerization to prepare high
572 performance thin film composite reverse osmosis membranes based on hydrophilic
573 supports, Polymer, 144 (2018) 159-167.
574 [27] M. Shi, W. Yan, Y. Zhou, Z. Wang, L. Liu, S. Zhao, Y. Ji, J. Wang, C. Gao, P.
575 Zhang, X. Cao, Combining tannic acid-modified support and a green co-solvent for
576 high performance reverse osmosis membranes, J. Membr. Sci., 595 (2020).
577 [28] M. Hirose, H. Ito, Y. Kamiyama, Effect of skin layer surface structures on the flux
578 behaviour of RO membranes, J. Membr. Sci., 121 (1996) 209-215.
579 [29] X.-H. Ma, Z.-K. Yao, Z. Yang, H. Guo, Z.-L. Xu, C.Y. Tang, M. Elimelech,
580 Nanofoaming of Polyamide Desalination Membranes To Tune Permeability and
581 Selectivity, Environ. Sci. Technol. Lett., 5 (2018) 123-130.
582 [30] X. Ma, Z. Yang, Z. Yao, H. Guo, Z. Xu, C.Y. Tang, Tuning roughness features of
583 thin film composite polyamide membranes for simultaneously enhanced permeability,
584 selectivity and anti-fouling performance, J. Colloid Interface Sci., 540 (2019) 382-388.
585 [31] L.E. Peng, Z. Yao, X. Liu, B. Deng, H. Guo, C.Y. Tang, Tailoring Polyamide
586 Rejection Layer with Aqueous Carbonate Chemistry for Enhanced Membrane
587 Separation: Mechanistic Insights, Chemistry-Structure-Property Relationship, and
588 Environmental Implications, Environ. Sci. Technol., 53 (2019) 9764-9770.
589 [32] B. Ukrainsky, G.Z. Ramon, Temperature measurement of the reaction zone during
590 polyamide film formation by interfacial polymerization, J. Membr. Sci., 566 (2018) 329-
591 335.
592 [33] X. Song, B. Gan, Z. Yang, C.Y. Tang, C. Gao, Confined nanobubbles shape the
593 surface roughness structures of thin film composite polyamide desalination
594 membranes, J. Membr. Sci., 582 (2019) 342-349.
595 [34] L.E. Peng, Z. Yao, Z. Yang, H. Guo, C.Y. Tang, Dissecting the Role of Substrate
596 on the Morphology and Separation Properties of Thin Film Composite Polyamide
597 Membranes: Seeing Is Believing, Environ. Sci. Technol., 54 (2020) 6978-6986.
598 [35] G.-Y. Chai, W.B. Krantz, Formation and characterization of polyamide membranes
599 via interfacial polymerization, J. Membr. Sci., 93 (1994) 175-192.
600 [36] J. Xu, H. Yan, Y. Zhang, G. Pan, Y. Liu, The morphology of fully-aromatic
601 polyamide separation layer and its relationship with separation performance of TFC
602 membranes, J. Membr. Sci., 541 (2017) 174-188.
603 [37] Q. Zhang, Z. Zhang, L. Dai, H. Wang, S. Li, S. Zhang, Novel insights into the
604 interplay between support and active layer in the thin film composite polyamide

membranes, J. Membr. Sci., 537 (2017) 372-383.
[38] J. Wang, R. Xu, F. Yang, J. Kang, Y. Cao, M. Xiang, Probing influences of support layer on the morphology of polyamide selective layer of thin film composite membrane, J. Membr. Sci., 556 (2018) 374-383.
[39] S.H. Yalkowsky, Y. He, P. Jain, Handbook of aqueous solubility data, CRC press, 2016.
[40] X. Zhu, Z. Yang, Z. Gan, X. Cheng, X. Tang, X. Luo, D. Xu, G. Li, H. Liang, Toward tailoring nanofiltration performance of thin-film composite membranes: Novel insights into the role of poly(vinyl alcohol) coating positions, J. Membr. Sci., 614 (2020).
[41] X. Zhu, X. Cheng, X. Luo, Y. Liu, D. Xu, X. Tang, Z. Gan, L. Yang, G. Li, H. Liang, Ultrathin Thin-Film Composite Polyamide Membranes Constructed on Hydrophilic Poly(vinyl alcohol) Decorated Support Toward Enhanced Nanofiltration Performance, Environ. Sci. Technol., 54 (2020) 6365-6374.
[42] S.H. Yun, P.G. Ingole, K.H. Kim, W.K. Choi, J.H. Kim, H.K. Lee, Properties and performances of polymer composite membranes correlated with monomer and polydopamine for flue gas dehydration by water vapor permeation, Chem. Eng. J., 258 (2014) 348-356.
[43] L. Xia, J. Ren, M. Weyd, J.R. McCutcheon, Ceramic-supported thin film composite membrane for organic solvent nanofiltration, J. Membr. Sci., 563 (2018) 857-863.
[44] W. Xie, G.M. Geise, B.D. Freeman, H.-S. Lee, G. Byun, J.E. McGrath, Polyamide interfacial composite membranes prepared from m-phenylene diamine, trimesoyl chloride and a new disulfonated diamine, J. Membr. Sci., 403-404 (2012) 152-161.
[45] H. Karimi, M. Bazrgar Bajestani, S.A. Mousavi, R. Mokhtari Garakani, Polyamide membrane surface and bulk modification using humid environment as a new heat curing medium, J. Membr. Sci., 523 (2017) 129-137.
[46] Z.-M. Zhan, Z.-L. Xu, K.-K. Zhu, Y.-J. Tang, How to understand the effects of heat curing conditions on the morphology and performance of polypiperazine-amide NF membrane, J. Membr. Sci., 597 (2020).
[47] Z. Jiang, S. Karan, A.G. Livingston, Water Transport through Ultrathin Polyamide Nanofilms Used for Reverse Osmosis, Adv. Mater., 30 (2018) 1705973.
[48] Y. Wen, X. Zhang, X. Li, Z. Wang, C.Y. Tang, Metal–Organic Framework Nanosheets for Thin-Film Composite Membranes with Enhanced Permeability and Selectivity, ACS Applied Nano Materials, (2020).
[49] Z. Yang, F. Wang, H. Guo, L.E. Peng, X.H. Ma, X.X. Song, Z. Wang, C.Y. Tang, Mechanistic Insights into the Role of Polydopamine Interlayer toward Improved

640 Separation Performance of Polyamide Nanofiltration Membranes, Environ. Sci.
641 Technol., 54 (2020) 11611-11621.
642 [50] I. Smallwood, Handbook of organic solvent properties, Butterworth-Heinemann,
643 2012.
644 [51] X. Song, B. Gan, S. Qi, H. Guo, C.Y. Tang, Y. Zhou, C. Gao, Intrinsic Nanoscale
645 Structure of Thin Film Composite Polyamide Membranes: Connectivity, Defects, and
646 Structure-Property Correlation, Environ. Sci. Technol., 54 (2020) 3559-3569.
647 [52] J. Muscatello, E.A. Müller, A.A. Mostofi, A.P. Sutton, Multiscale molecular
648 simulations of the formation and structure of polyamide membranes created by
649 interfacial polymerization, J. Membr. Sci., 527 (2017) 180-190.
650 [53] A.S. Al-Hobaib, M.S. Al-Suhybani, K.M. Al-Sheetan, H. Mousa, M.R. Shaik, New
651 RO TFC Membranes by Interfacial Polymerization in n-Dodecane with Various co-
652 Solvents, Membranes (Basel), 6 (2016).
653 [54] X. Song, S. Qi, C.Y. Tang, C. Gao, Ultra-thin, multi-layered polyamide membranes:
654 Synthesis and characterization, J. Membr. Sci., 540 (2017) 10-18.
655 [55] B.H. Jeong, E.M.V. Hoek, Y.S. Yan, A. Subramani, X.F. Huang, G. Hurwitz, A.K.
656 Ghosh, A. Jawor, Interfacial polymerization of thin film nanocomposites: A new concept
657 for reverse osmosis membranes, J. Membr. Sci., 294 (2007) 1-7.
658 [56] J.E. Gu, S. Lee, C.M. Stafford, J.S. Lee, W. Choi, B.Y. Kim, K.Y. Baek, E.P. Chan,
659 J.Y. Chung, J. Bang, J.H. Lee, Molecular layer-by-layer assembled thin-film composite
660 membranes for water desalination, Adv. Mater., 25 (2013) 4778-4782.
661